

Carotenoid Radical Formation: Dependence on Conjugation Length

A. Ligia Focsan,[†] Michael K. Bowman,[†] Péter Molnár,[‡] József Deli,[§] and Lowell D. Kispert*,[†]

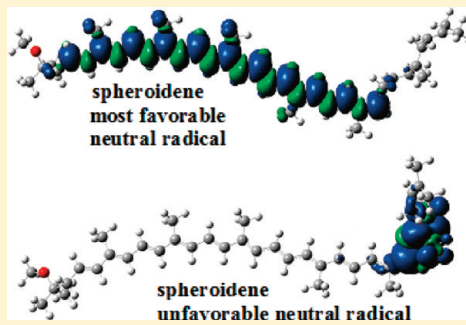
[†]Department of Chemistry, The University of Alabama, Tuscaloosa, Alabama 35487-0336, United States

[‡]Department of Pharmacognosy, University of Pécs, Medical School, H-7624 Pécs, Rókus u. 2, Pécs, Hungary

[§]Department of Biochemistry and Medical Chemistry, University of Pécs, Medical School, H-7624 Pécs, Szigeti út 12, Pécs, Hungary

Supporting Information

ABSTRACT: The relative energy of carotenoid neutral radicals formed by proton loss from the radical cations of linear carotenoids has been examined as a function of conjugation length from $n = 15$ to 9. For a maximum conjugation length of $n = 15$ (bisdehydrolycopenes, a symmetrical compound), proton loss can occur from any of the 10 methyl groups, with proton loss from the methyl group at position C1 or C1' being the most favorable. In contrast, the most energetically favorable proton loss from the radical cations of lycopene, neurosporene, spheroidene, spheroidenone, spirilloxanthin, and anhydrorhodovibrin occurs from methylene groups that extend from the conjugated system. For example, decreasing the conjugation length to $n = 11$ (lycopene) by saturation of the double bonds C3–C4 and at C3'–C4' of bisdehydrolycopenes favors proton loss at C4 or C4' methylene groups. Saturation at C7'–C8' in the case of neurosporene, spheroidene, and spheroidenone ($n = 9, 10, 11$) favors the formation of a neutral radical at the C8' methylene group. Saturation of C1–C2 by addition of a methoxy group to a bisdehydrolycopenes-like structure with conjugation of $n = 12$ or 13 (anhydrorhodovibrin, spirilloxanthin) favors proton loss at the C2 methylene group. As a consequence of deprotonation of the radical cation, the unpaired electron spin distribution changes so that larger β -methyl proton couplings occur for the neutral radicals (13–16 MHz) than for the radical cation (7–10 MHz), providing a means to identify possible carotenoid radicals in biological systems by Mims ENDOR.



INTRODUCTION

Photosynthesis in green plants involves extensive use of xanthophylls, which are carotenoids with terminal cyclohexene rings. The photosynthetic bacteria, however, rely on linear carotenoids, some of which are represented in Scheme 1. The radical cation of xanthophylls and subsequent deprotonation products are increasingly implicated as having an important role in green plants, but much less attention has been paid to similar roles for the linear carotenoids of bacterial photosynthesis.

The conjugation length of the carotenoids is an important factor in light-harvesting complexes, in energy transfer, under the growth conditions of bacteria, and in the formation of radicals. For example, the crystal structure of the light-harvesting complex 2 (LH2) from *Rhodospirillum (Rs.) molischianum*¹ shows that the major carotenoid, all-trans lycopene (**II** in Scheme 1) has one end near the surface of the membrane, whereas the other end is buried in the hydrophobic core in contact with bacteriochlorophylls. It was concluded that the van der Waals contact of lycopene and bacteriochlorophylls *a* (BChl-*a*) in LH2 enables singlet and triplet energy transfer via the Dexter mechanism.¹ However, there was no consideration of lycopene radical cation formation and its deprotonation.

There is very specific binding of carotenoids to reaction center (RC) or light harvesting complex.² Spirilloxanthin **VII** with conjugation length $n = 13$ was always preferentially bound to the RC and anhydrorhodovibrin **VI** ($n = 12$) to light-harvesting

complex I (LH1) of *Rhodobium marinum*. In *Rubrivivax gelatinosus*, **VII** was preferentially bound to RC, whereas neurosporene **III** ($n = 9$) and spheroidene **IV** ($n = 10$) were preferentially bound to LH2.

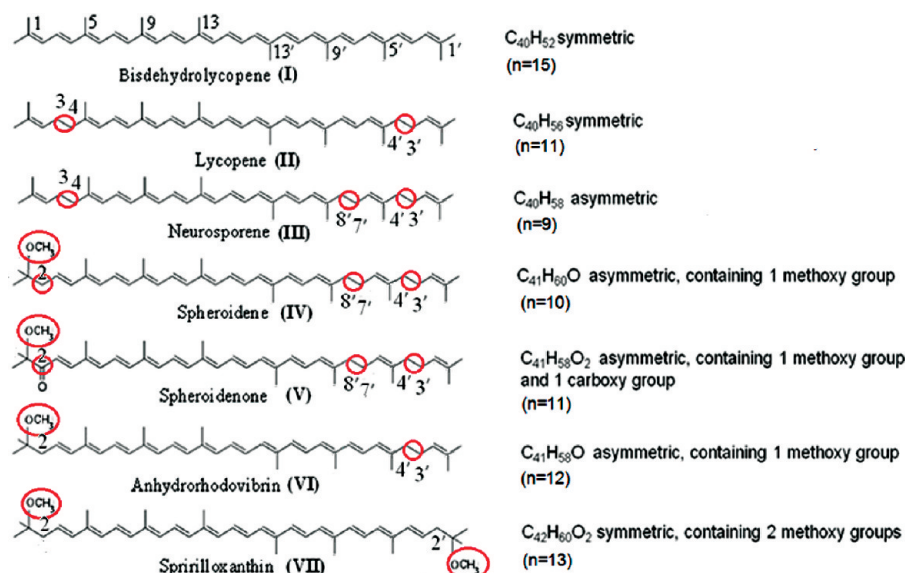
In *Rhodobacter (Rb.) sphaeroides* 2.4.1,³ spheroidene **IV** and spheroidenone **V** are differentially synthesized depending on growth conditions: **IV** occurs during growth under anaerobic conditions and low light intensities and associated with the B800–850 complex, whereas **V** predominates during anaerobic growth at high light intensities and is more abundant in the B875 complex. It is inferred that conversion of **IV** to **V** (conjugation length increases from $n = 10$ to 11) might play a significant role in adaptation to changes in light intensity. Later, the effect of the conjugation length of carotenoids on the S₁-mediated carotenoid to BChl-*a* energy-transfer pathway and carotenoid radical formation was examined⁴ for a series of LH2 complexes from *Rb. sphaeroides*. S₁-mediated energy transfer was 94, 82, and 76%, respectively, for **III**, **IV**, and **V**. The yield of carotenoid radicals was highest for **III** (10–15%), lower for **IV** (5–8%), and zero for **V**, suggesting that in the LH2 complex the carotenoid radicals are formed with higher efficiency for shorter conjugation length. This dependence for radical cation formation was later

Received: May 23, 2011

Revised: June 27, 2011

Published: June 28, 2011

Scheme 1. Linear Carotenoids



explained by computing the potential energy surfaces for the excited-state properties of various $\text{Car}^{+}\cdots\text{BChl}^{+}$ charge transfer complexes.⁵ It was determined that the charge transfer state is below the S1 state for III, degenerate with that for IV, and above the S1 state for V, thus preventing population of the charge transfer state and formation of radicals for V. A Raman spectroscopic study of LH2 from *Rb. sphaeroides*⁶ deduced that carotenoids III, IV, and V sit with the polar ends embedded inside the protein in the vicinity of the B850 BChl molecules. However, the initial crystal structure of LH2 from *Rhodopseudomonas (Rps.) acidophila* 10050 shows the polar end of the carotenoid in a hydrophilic pocket at the surface of the membrane, whereas the nonpolar other end is close (3.62 Å) to Bchl B850.⁷ Refinement of the crystal structure^{8,9} confirms the orientation⁷ and also reveals a second set of carotenoids in contact with Bchl B850 and inserted from the opposite side of the membrane. Every carotenoid is oriented with its polar end at a membrane surface.

Charge-transfer complexes form between carotenoid and chlorophyll, $\text{Car}^{+}\cdots\text{Chl}^{-}$, which have been shown to be involved in nonphotochemical quenching.¹⁰ The charge-transfer quenching mechanism was proposed as a result of detecting a radical cation of zeaxanthin in the thylakoid membrane of higher plants.¹⁰ Study of the carotenoid radical cations is imperative to better understand the processes in which they actively participate and why conjugation length plays such a role in energy transfer and in formation of neutral radicals generated in both artificial matrices^{11–13} and in photosystem II¹⁴ by proton loss from the radical cation. A carotenoid neutral radical would be very efficient in quenching chlorophyll's excess energy, analogous to fluorescence quenching by free radicals.¹⁵ The expected ability to form relatively long-lived neutral radicals of the four carotenoids present in LH2 is highly correlated with their quenching or nonquenching role: zeaxanthin and lutein radical cations, known quenchers, allow formation of neutral radicals through proton loss at the terminal rings; violaxanthin and 9'-*cis*-neoxanthin, known as nonquenchers, cannot form neutral radicals from the radical cations because groups on the terminal rings block the proton loss. The terminal rings are in a polar environment near

the surface of the membrane in contact with the aqueous environment outside the membrane. This environment would readily accept protons from the terminal rings of zeaxanthin and lutein radical cations whose pK_a values range between 4 and 7. Proton loss from the methyl groups situated on the polyene chain is energetically unfavorable for all four carotenoids. In addition, the nonpolar environment that surrounds the polyene chains of the carotenoids hinders the proton loss.¹¹

In this Article, we turn our attention to the linear carotenoids (Scheme 1) and the role that conjugation length plays in the formation of radical cations and neutral radicals. We examine in detail the symmetric model compound bisdehydrolycopen I ($n = 15$ conjugated double bonds) II ($n = 11$), and VII ($n = 13$) and the asymmetric III ($n = 9$), IV ($n = 10$), V ($n = 11$), and VI ($n = 12$). (See Scheme 1.)

METHODS

DFT Calculations. DFT calculations were done with the Gaussian 03 program package¹⁶ on the Cray XD1 computer at the Alabama Supercomputer Center. Geometries were optimized at the B3LYP/6-31G** level,^{17,18} which we have previously shown¹⁹ to be suitable for predicting the geometry of β -carotene-based radicals. Single-point calculations at these geometries were used to predict hyperfine couplings at the B3LYP level with the TZP basis set from the Ahlrich's group.²⁰ This basis set gives good NMR chemical shifts²¹ and EPR parameters that agree well with the experimental data for carotenoids.^{12,19} The proton hyperfine couplings calculated with this method are within 0.5 MHz of the experimental couplings, whereas other levels of theory give values that differ by as much as a factor of 2. The unpaired spin densities were obtained using the AGUI interface (Semichem)²² from the wave functions and spin densities produced by Gaussian 03. The unpaired spin density is defined as the difference in the α and β spin densities.

Pulsed ENDOR Measurements. Pulsed ENDOR experiments were carried out with a Bruker ELEXSYS E-680W/XFT/CW pulse X-band EPR spectrometer with an ENI A-500 RF power

a, b

^a Delocalization N is given under each $\Delta E(n)$ value and indicated by a parenthesis. ^b Note: $\Delta E(n)$ is calculated relative to the energy minimum; delocalization is estimated by counting the number of C atoms over which significant spin (>0.002) is delocalized in Figures 1–7.

amplifier using the Mims ($\pi/2-\tau-\pi/2-T-\pi/2-\tau$ -echo) pulse sequences with a RF π -pulse applied during the delay time, T .²³ Pulsed ENDOR simulations were performed using the SimBud/SpecLab programs²⁴ using hyperfine coupling tensors obtained from DFT calculations. Simulations of the individual couplings were summed and processed using the SpecLab program.

■ RESULTS

Most Favorable Neutral Radicals. In Table 1 are given the relative energies $\Delta E(n)$ for the neutral radicals $\#Car^\bullet(n)$ formed by proton loss ($\#$ indicates proton loss at position n) from the carotenoid radical cations $Car^{+\bullet}$ of various linear carotenoids. The relative energy for proton loss varies up to 18.5 kcal/mol. The relative energy varies inversely to the delocalization length. In all cases, except bisdehydrolycopenene, the most favorable deprotonation site is at a methylene group of the radical cation that extends the unpaired spin delocalization length, and these sites are discussed next.

Bisdehydrolycopenene (**I**), a linear, symmetric carotenoid that has 10 methyl groups in 4 distinct positions, C1(1'), C5(5'), C9(9'), and C13(13') (Scheme 1), was used as reference model because of the fully conjugated chain with conjugation length $n = 15$. For its radical cation $\mathbf{I}^{\bullet+}$, proton loss is feasible from all 10 methyl groups, with a preference for loss at C1(1'). (See Table 1.)

However, decreasing the conjugation length to $n = 11$ (see lycopene **II** in Scheme 1) by saturating the C3–C4 (circled) and C3'–C4' (circled) double bonds at each end, makes proton loss at C4 and C4' methylene groups most favorable. The addition of two protons at C7'–C8' (circled) to decrease the conjugation length $n = 9$ (see neurosporene **III**) makes proton loss from the methylene group C8' essentially isoenergetic with proton loss from the C4 methylene group.

Moving the double bond from C1–C2 of III to C3–C4 and adding a methoxy group to C1 forms a $n = 10$ conjugated system (see spheroidene IV) where proton loss is favored from C2 (circled) or from C8'. Adding a carbonyl group at position C2 (circled) of IV generates a $n = 11$ conjugated system (see spheroidenone V) but prevents loss from C2 so that favorable loss occurs only at C8' position.

For $n = 12$ (see anhydrorhodovibrin VI), adding a double bond to IV at C7'-C8' (circled) prevents proton loss at this position. The most favorable sites of proton loss are C2 and C4'. Methoxy addition at C1 and C1' (circled) of I gives rise to a symmetrical molecule with $n = 13$ (see spirilloxanthin VII), for which loss is heavily favored from the C2 position or by symmetry at C2'.

Proton Loss From the Methyl Groups. For I, the relative energies for loss of proton at the methyl groups at C5(5') to C9(9') to C13(13') are less favorable by 8 to 9 kcal/mol than that at the C1(1')-methyl group. (See Table 1.) The relative energies for proton loss from the methyl groups of II also increase from C5(5'), C9(9'), to C13(13'), and they are higher than the minimum energy by 5.28, 11.01, and 11.33 kcal/mol, respectively. Breaking the symmetry to form III for the primed half of the molecule makes proton loss at C9' and C5-methyl groups more favorable, followed by loss at C9', C13' and C13 methyl groups. For carotenoids IV and V, proton loss from C9' is the most favorable at C9'. Adding a double bond to the structure of III at position C3-C4 to extend conjugation to $n = 10$ and 11

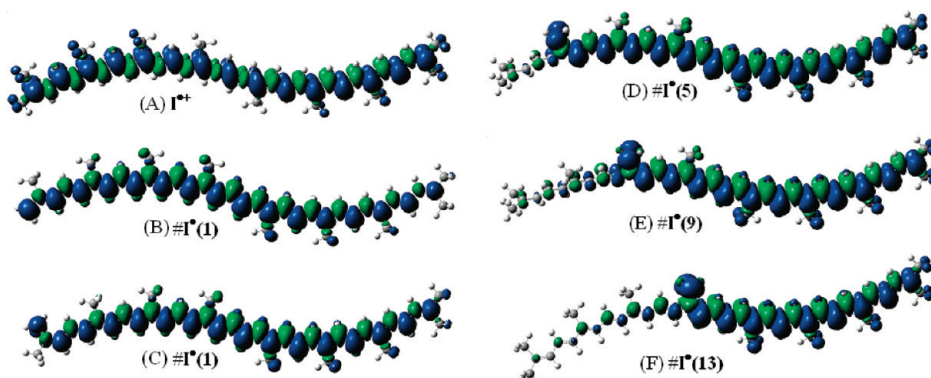


Figure 1. Unpaired spin density distribution for bisdehydrolycopenes radicals: (A) I''^+ , (B) $\#\text{I}'(1)$ *cis*, (C) $\#\text{I}'(1)$ *trans*, (D) $\#\text{I}'(5)$, (E) $\#\text{I}'(9)$, and (F) $\#\text{I}'(13)$ from DFT calculations.

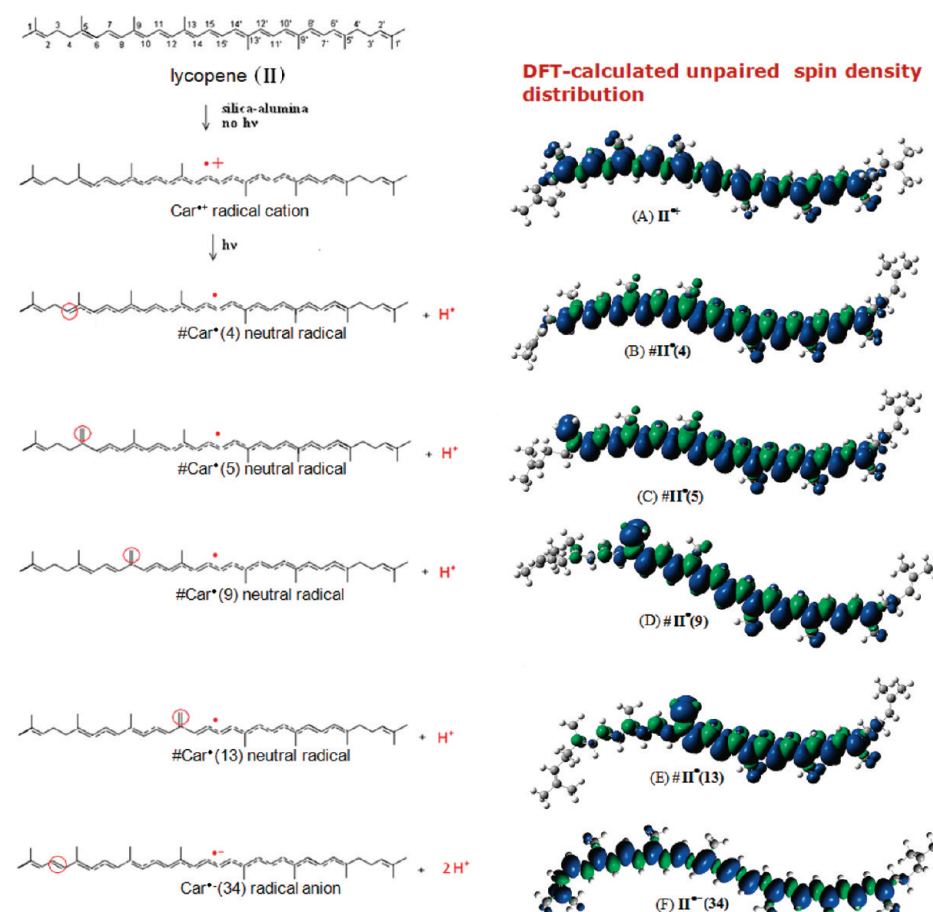


Figure 2. Possible intermediates for lycopene (II); Unpaired spin density distribution for lycopene radicals: (A) II''^+ , (B) $\#\text{II}'(4)$, (C) $\#\text{II}'(5)$, (D) $\#\text{II}'(9)$, (E) $\#\text{II}'(13)$, and (F) $\text{II}''^-(34)$ from DFT calculations.

(carotenoids IV and V respectively, see Scheme 1) makes proton loss at C5 less favorable when compared with II and III (~ 5 kcal/mol higher). (See Table 1.) Also, proton loss at C9' is less favorable for V (~ 4 kcal/mol higher) when compared with III and IV. For VI and VII, the relative energies are comparable; however, proton loss from C5' is much more favorable in the case of VI (4.62 kcal/mol) than VII (9.55 kcal/mol).

Except for bisdehydrolycopen I, the most stable neutral radicals are those formed by proton loss from methylene groups

of the radical cations at the ends of the longest conjugated regions. Loss at these positions lengthens the region of delocalization. Proton loss from a methyl group is less favored by 4–13 kcal/mol. The most favored site for loss of a methyl group is one near the end of the longest conjugated region that results in the smallest decrease in conjugation length at C5, C5', or C9' methyl groups.

Unpaired Spin Density Distribution. The radical cations Car''^+ and neutral radicals $\#\text{Car}'(n)$ of linear carotenoids I–VII

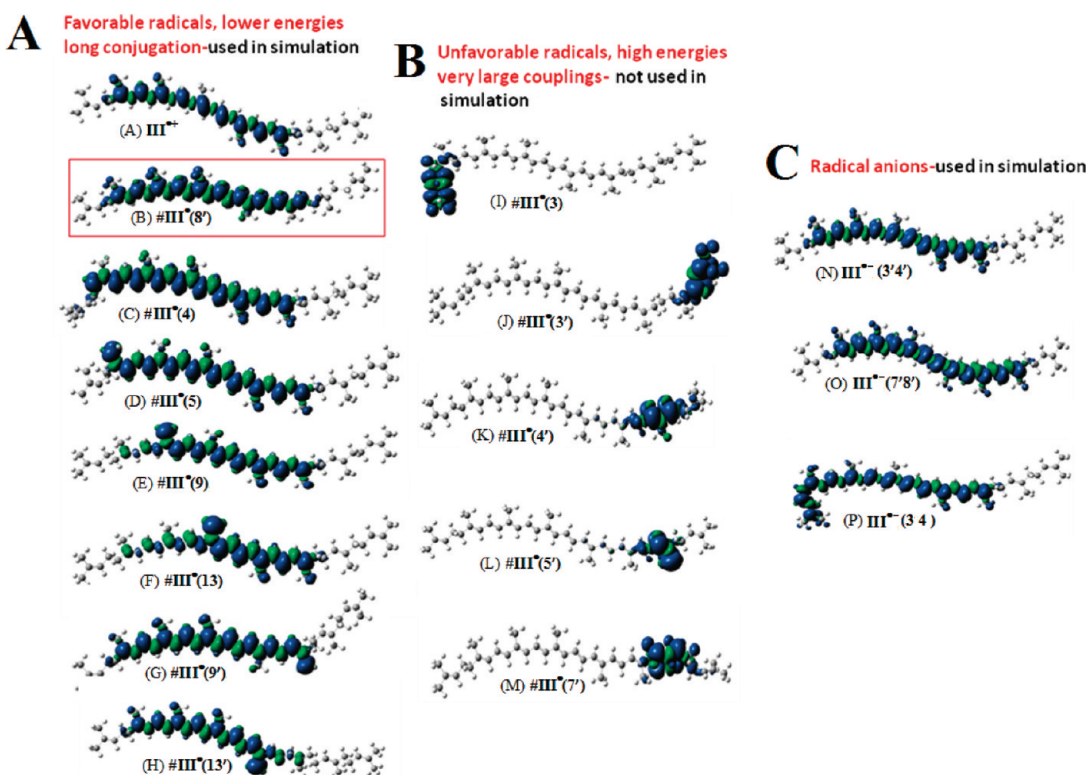


Figure 3. Unpaired spin density distribution for neurosporene: (A) $\text{III}^{\bullet+}$, (B) $\# \text{III}^{\bullet}(8')$, (C) $\# \text{III}^{\bullet}(4)$, (D) $\# \text{III}^{\bullet}(5)$, (E) $\# \text{III}^{\bullet}(9)$, (F) $\# \text{III}^{\bullet}(13)$, (G) $\# \text{III}^{\bullet}(9')$, (H) $\# \text{III}^{\bullet}(13')$, (I) $\# \text{III}^{\bullet}(3)$, (J) $\# \text{III}^{\bullet}(3')$, (K) $\# \text{III}^{\bullet}(4')$, (L) $\# \text{III}^{\bullet}(5')$, (M) $\# \text{III}^{\bullet}(7')$, (N) $\text{III}^{\bullet-}(3'4')$, (O) $\text{III}^{\bullet-}(7'8')$, and (P) $(\text{III}^{\bullet-}(34))$ from DFT calculations.

exhibit a spin pattern with alternating positive and negative lobes, as seen in Figures 1–7. The radical cation of I has the unpaired spin distributed all along the polyene chain from C1 to C1', whereas for the neutral radicals, the unpaired spin density increases on the side with longest conjugation and decreases on the other side (Figure 1). The length of delocalization of the spin density for the neutral radicals decreases consequently from $\# \text{I}^{\bullet}(1)$ to $\# \text{I}^{\bullet}(5)$ to $\# \text{I}^{\bullet}(9)$ to $\# \text{I}^{\bullet}(13)$, so the relative energies of the neutral radicals increase in the same direction. Indeed, $\# \text{I}^{\bullet}(1)$ has the lowest minimum energy among the neutral radicals formed and is more stable than $\# \text{I}^{\bullet}(5)$ by 7.83 kcal/mol, more stable than $\# \text{I}^{\bullet}(9)$ by 8.93 kcal/mol, and more stable than $\# \text{I}^{\bullet}(9')$ by 9.25 kcal/mol (Table 1). This pattern is repeated in the other linear carotenoids with much greater changes in relative energy.

For II, neutral radicals formed by proton loss at positions C4 and C4' have a longer delocalization length and lower energy (Table 1) than those formed by removing protons from the methyl groups (Figure 2). In the case of neurosporene III (Figure 3), the longest conjugated structure is formed for $\# \text{III}^{\bullet}(8')$ (Figure 3A), comparable to $\# \text{III}^{\bullet}(4)$ and followed by neutral radicals whose proton was lost from the methyl groups $\# \text{III}^{\bullet}(5)$, $\# \text{III}^{\bullet}(9)$, $\# \text{III}^{\bullet}(9')$, $\# \text{III}^{\bullet}(13)$, and $\# \text{III}^{\bullet}(13')$. For the neutral radicals $\# \text{III}^{\bullet}(3)$, $\# \text{III}^{\bullet}(3')$, $\# \text{III}^{\bullet}(4')$, $\# \text{III}^{\bullet}(5')$, and $\# \text{III}^{\bullet}(7')$ the unpaired spin is localized (four carbon atoms), giving rise to structures with relative energies 11.5 to 16 kcal/mol higher and very large hyperfine couplings as large as 30–70 MHz (I–M in Figure 3B). IV and V radical cations form neutral radicals very similar to those of III. High-energy structures with unpaired spin density localized (~ 4 carbon atoms) and very large hyperfine couplings also form in the case of IV and V. (See Figures 4 F–I and 5 E–H.)

Loss of a proton from position C2 and C4' of VI (Figure 6) and positions C2(2') of VII (Figure 7) generates the most energetically favorable neutral radicals with the longest conjugation length, followed by the neutral radicals formed by proton loss from the methyl groups C5(5'), C9(9'), and C13(13'), respectively, with relative energies on the same order of magnitude and similar isotropic hyperfine coupling constants as large as 15 MHz.

In summary, radical cations have smaller hyperfine coupling constants than the neutral radicals; low-energy neutral radicals have larger couplings, and high-energy radicals have very large couplings and localized unpaired spin distribution. (See Tables S1–S66 in the Supporting Information for the hyperfine coupling tensors for each radical of carotenoids I–VII.)

Simultaneous loss of two protons from position C3–C4 of $\text{II}^{\bullet+}$ produces a radical anion $\text{II}^{\bullet-}(34)$ (Figure 2F) with the unpaired spin distributed over the entire conjugation length. Simultaneous proton loss at positions C3–C4, C3'-C4', and C7'-C8' is also possible for III, forming the radical anions $\text{III}^{\bullet-}(34)$, $\text{III}^{\bullet-}(3'4')$, and $\text{III}^{\bullet-}(7'8')$ (N–P in Figure 3C). $\text{III}^{\bullet-}(7'8')$ is a radical anion with isotropic couplings as large as 6.8 MHz (Table S28 in the Supporting Information), similar to those of the radical cation of lycopene. Proton loss at 3–4 positions extends the conjugation, whereas proton loss at the opposite side of the molecule at 3'-4' positions has no effect on it, making the unpaired spin distribution similar to the radical cation of neurosporene. (See Figure 3C.) For IV, V, and VI, it is possible to form radical anions by simultaneous loss at C3'-C4' positions, C7'-C8' positions, or both. In general, the hyperfine couplings of the radical anions are very similar to those of the corresponding radical cation.

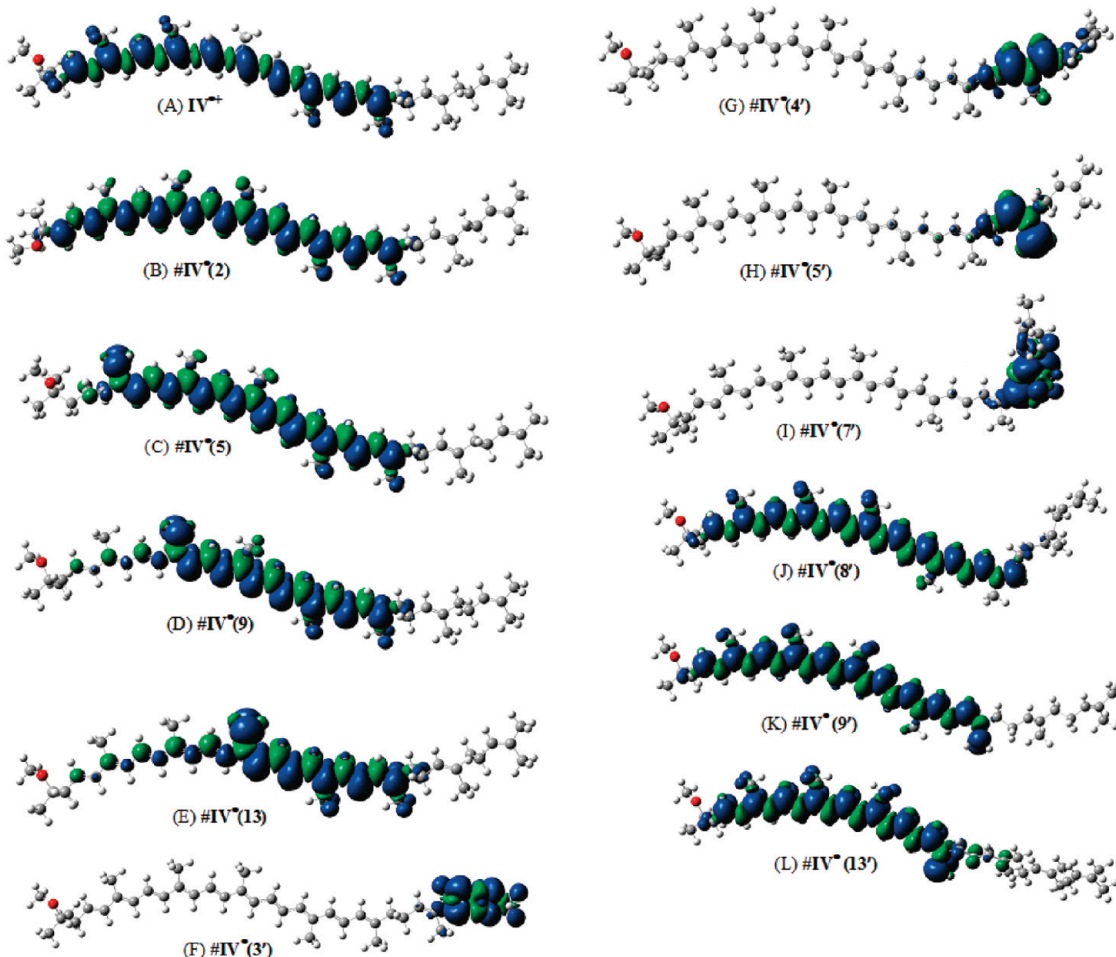


Figure 4. Unpaired spin density distribution for spheroidene radicals: (A) $\text{IV}^{\bullet+}$, (B) $\text{IV}^{\bullet}(2)$, (C) $\# \text{IV}^{\bullet}(5)$, (D) $\# \text{IV}^{\bullet}(9)$, (E) $\# \text{IV}^{\bullet}(13)$, (F) $\# \text{IV}^{\bullet}(3')$, (G) $\# \text{IV}^{\bullet}(4')$, (H) $\# \text{IV}^{\bullet}(5')$, (I) $\# \text{IV}^{\bullet}(7')$, (J) $\# \text{IV}^{\bullet}(8')$, (K) $\# \text{IV}^{\bullet}(9')$, and (L) $\# \text{IV}^{\bullet}(13')$ from DFT calculations.

Dependence of ΔE on Delocalization. For each carotenoid, there is a smooth relationship between relative energy, $\Delta E(n)$, and delocalization length, N , over which the unpaired spin density is distributed. (See Figure S1 in the Supporting Information, where $\Delta E(n)$ is plotted versus N using the values in Table 1.) Notably, by plotting the relative energy, $\Delta E(n)$, versus the change in delocalization length, $N - N_{\max}$, the values of $\Delta E(n)$ for all radicals fall near a line depicted in Figure 8. The $\Delta E(n)$ changes rapidly as $N - N_{\max}$ decreases until it reaches a constant value of ~ 12 kcal/mol. The exception is I (indicated by black dots), which is the only carotenoid examined that contains no methylene groups.

Mims ENDOR Spectra. The difference in unpaired spin density provides a possible opportunity to use ENDOR to detect the presence of neutral radicals of the linear carotenoids in the same fashion as for the xanthophylls.^{11–13,25,26} DFT-calculated isotropic and anisotropic proton hyperfine coupling constants for different carotenoid radicals are accurate enough¹⁹ to be used in simulation and interpretation of overlapping powder ENDOR spectra composed of a mixture of carotenoid radicals.^{11,13} Simulated spectra for xanthophylls found signatures for the presence of the radical cation $\text{Car}^{\bullet+}$ as well as the presence of carotenoid neutral radicals, $\# \text{Car}^{\bullet}(n)$.

DFT calculations of carotenoid radical cations containing cyclohexene rings such as β -carotene^{14,19} and the xanthophylls

zeaxanthin,¹² violaxanthin,¹² lutein,¹³ astaxanthin,²⁵ canthaxanthin,²⁶ and 9'-*cis* neoxanthin¹¹ predicted isotropic β -methyl proton couplings < 10 MHz. The largest couplings correspond to C9 or C9' methyl groups. (See Table 2.) For linear carotenoids I, II, VI, and VII, these β -methyl couplings are smaller, ~ 7 MHz, and they correspond to C5 or C5' methyl groups. (See Table 2.) Larger isotropic hyperfine couplings of ~ 10 MHz occur for the radical cations of the linear carotenoids III, IV, and V, and they correspond to both C5 and C9' methyl groups.

Deprotonation produces larger β -methyl proton couplings for the neutral radicals than for the radical cation, which permits their identification in mixtures using Mims ENDOR. DFT calculations showed that carotenoid neutral radicals have methyl proton couplings of 13–16 MHz. The largest DFT-predicted isotropic β -methyl proton couplings for the neutral radicals are ~ 16 MHz (Table 2), in accord with pulsed Mims ENDOR measurements.^{11,13} The largest DFT-predicted isotropic coupling corresponds to the C13' methyl group of the neutral radical $\# \text{Car}^{\bullet}(13)$ for all studied carotenoids. (See Table 2.) Lines occurring above 19 MHz in previous ENDOR spectra were due to the anisotropic α -protons of the neutral radicals. The complete hyperfine coupling tensors for the radical cations, neutral radicals, and anion radicals for carotenoids I–VII are given in the Supporting Information as Tables S1–S66.

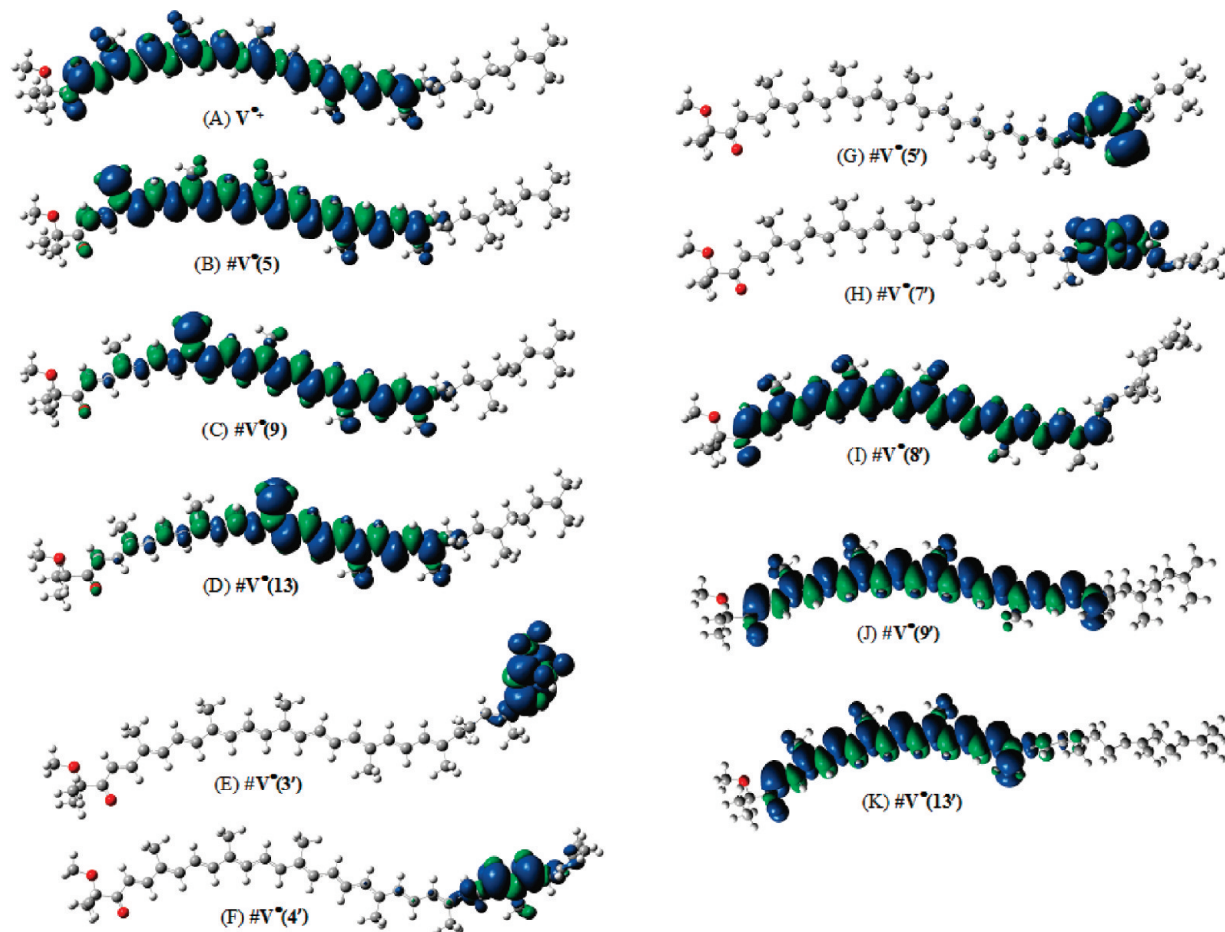


Figure 5. Unpaired spin density distribution for spheroidenone radicals: (A) $\text{V}^{\bullet+}$, (B) $\#\text{V}^{\bullet}(5)$, (C) $\#\text{V}^{\bullet}(9)$, (D) $\#\text{V}^{\bullet}(13)$, (E) $\#\text{V}^{\bullet}(3')$, (F) $\#\text{V}^{\bullet}(4')$, (G) $\#\text{V}^{\bullet}(5')$, (H) $\#\text{V}^{\bullet}(7')$, (I) $\#\text{V}^{\bullet}(8')$, (J) $\#\text{V}^{\bullet}(9')$, and (K) $\#\text{V}^{\bullet}(13')$ from DFT calculations.

Table 2. Largest Isotropic Coupling Constants from DFT Calculations for $\text{Car}^{\bullet+}$ and $\#\text{Car}^{\bullet}(n)$ (n Indicates the Position of Proton Loss)

carotenoid	$\text{Car}^{\bullet+}$ largest isotropic coupling	$\#\text{Car}^{\bullet}(13)$ largest isotropic coupling
β -carotene ^{14,19}	7.05 (C9)/7.05 (C9')	15.87 (C13')
zeaxanthin ¹²	8.33(C9)/8.26 (C9')	16.10 (C13')
violaxanthin ¹²	9.93 (C9)/10.00 (C9')	16.38 (C13')
lutein ¹³	8.04 (C9)/8.94 (C9')	16.35 (C13')
astaxanthin ²⁵	9.17 (C9)/9.23 (C9')	15.93 (C13')
canthaxanthin ²⁶	9.34 (C9)/9.36 (C9')	16.04 (C13')
9'- <i>cis</i> -neoxanthin ¹¹	10.41 (C9)/12.11 (C9')	16.76 (C13')
bisdehydrolycopen (I)	7.26 (C5)/7.26 (C5')	14.19 (C13')
lycopene (II)	7.84 (C5)/7.95 (C5')	15.57 (C13')
neurosporene (III)	10.9 (C5)/10.3 (C9')	16.86 (C13')
spheroidene (IV)	8.76 (C5)/10.3 (C9')	16.91 (C13')
spheroidenone (V)	10.63(C5)/9.74(C9')	16.82 (C13')
anhydrorhodovibrin (VI)	7.58 (C5)/7.54 (C5')	15.59 (C13')
spirilloxanthin (VII)	7.12 (C5)/7.09 (C5')	14.44 (C13')

In Figure 9 A, as an example, is given the simulations of individual contribution of VII radicals (indicated by the different colored spectra) to the Mims spectrum using the hyperfine

coupling tensors listed in the Supporting Information. If the DFT-generated hyperfine couplings for the radical cation VII^{•+} are used to simulate the Mims ENDOR spectrum using $\tau = 200$ ns, then these couplings would contribute to the middle part of the spectrum (shaded gray area under the black line in Figure 9A). Each of the favored neutral radicals #VII[•](2 and 2'), #VII[•](5 and 5'), #VII[•](9 and 9'), and #VII[•](13 and 13') contributes to the outer edges of the ENDOR spectrum <7.5 MHz and >22.5 MHz, whereas the radical cation does not. This makes the outer regions diagnostic for the presence of any of the favored neutral radicals. In Figure 9B is given the simulation of the sum of all individual radicals given in Figure 9A.

The neutral radicals of linear carotenoids, similarly to xanthophylls, can be detected from resolved peaks in the Mims ENDOR spectrum because of their much larger β -methyl proton couplings (of ~ 16 MHz). DFT can also be used to predict the spectra of radical anions that can form by simultaneous loss of two protons. Mims ENDOR spectra simulated for the linear carotenoid III indicate that the radical anions do not interfere with the detection of neutral radicals. For example, the Mims ENDOR simulation spectrum of neurosporene radical anions (Figure 10 in green) III^{•-}(34), III^{•-}(3'4'), and III^{•-}(7'8') in 1:1:1 ratio using the DFT-generated couplings (Tables S26–S28 in the Supporting Information) and $\tau = 220$ ns shows that the isotropic couplings, as high as 8 MHz, are slightly smaller than

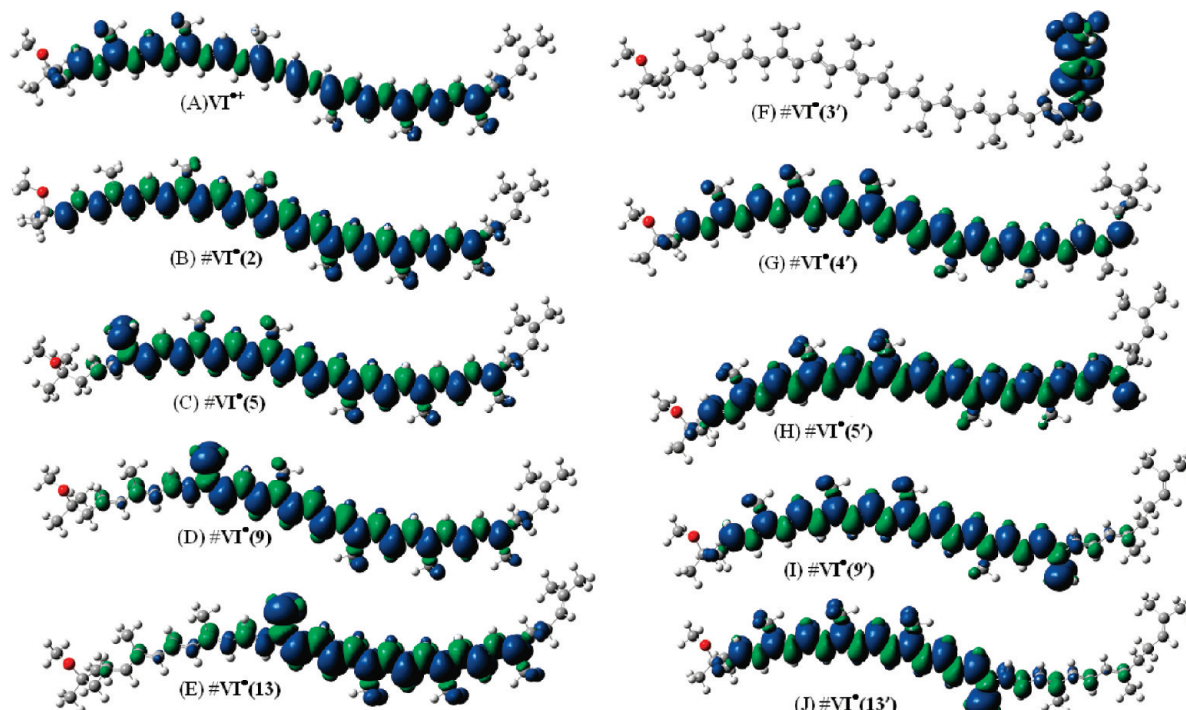


Figure 6. Unpaired spin density distribution for anhydrorhodovibrin radicals: (A) $\text{VI}^{\bullet+}$, (B) #VI $^{\bullet}(2)$, (C) #VI $^{\bullet}(5)$, (D) #VI $^{\bullet}(9)$, (E) #VII $^{\bullet}(13)$, (F) #VI $^{\bullet}(3')$, (G) #VI $^{\bullet}(4')$, (H) #VI $^{\bullet}(5')$, (I) #VI $^{\bullet}(9')$, and (J) #VI $^{\bullet}(13')$ from DFT calculations.

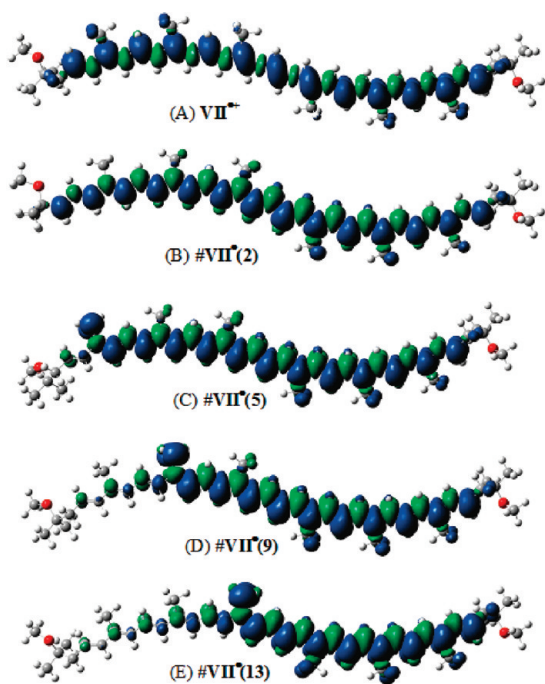


Figure 7. Unpaired spin density distribution for spirilloxanthin radicals: (A) VII $^{\bullet+}$, (B) #VII $^{\bullet}(2)$, (C) #VII $^{\bullet}(5)$, (D) #VII $^{\bullet}(9)$, and (E) #VII $^{\bullet}(13)$ from DFT calculations.

those of the radical cation (simulation in red), whereas the anisotropic couplings are as large as those of the radical cation, producing the peaks at the same positions. For the radical cation III $^{\bullet+}$ in red, both isotropic and anisotropic couplings are not larger than 11 MHz (Table S13 in the Supporting Information),

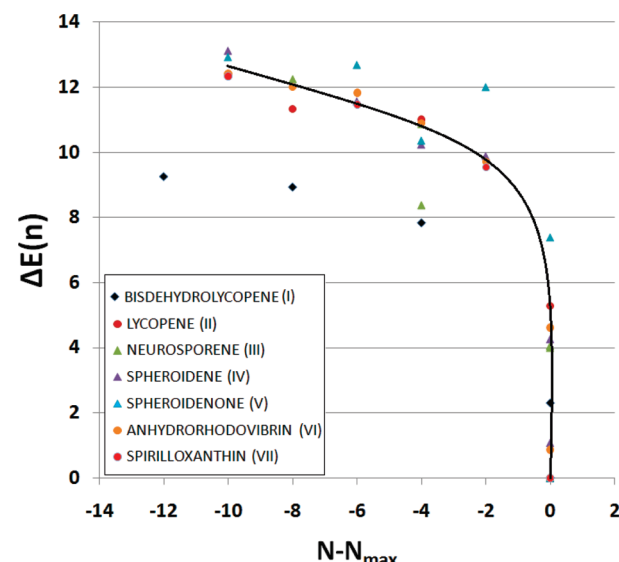


Figure 8. Relative energies ($\Delta E(n)$ in kilocalories per mole, Table 1) for loss of a proton from the radical cations versus relative change in delocalization $N - N_{\max}$ for I–VII. Smooth line has been drawn as a guide for the eye. Note: The localized neutral radicals having high relative energy and short conjugated chain (~ 4 C atoms) were not included.

the couplings giving rise to peaks centered at about 9.5 and 20.5 MHz, respectively. Simulation of the radical anions, radical cation, and all the favorable neutral radicals using the DFT-generated couplings gives rise to the spectrum in blue, which shows the exclusive contribution of the neutral radicals at the outer edges < 10 MHz and > 20 MHz, indicated by *.

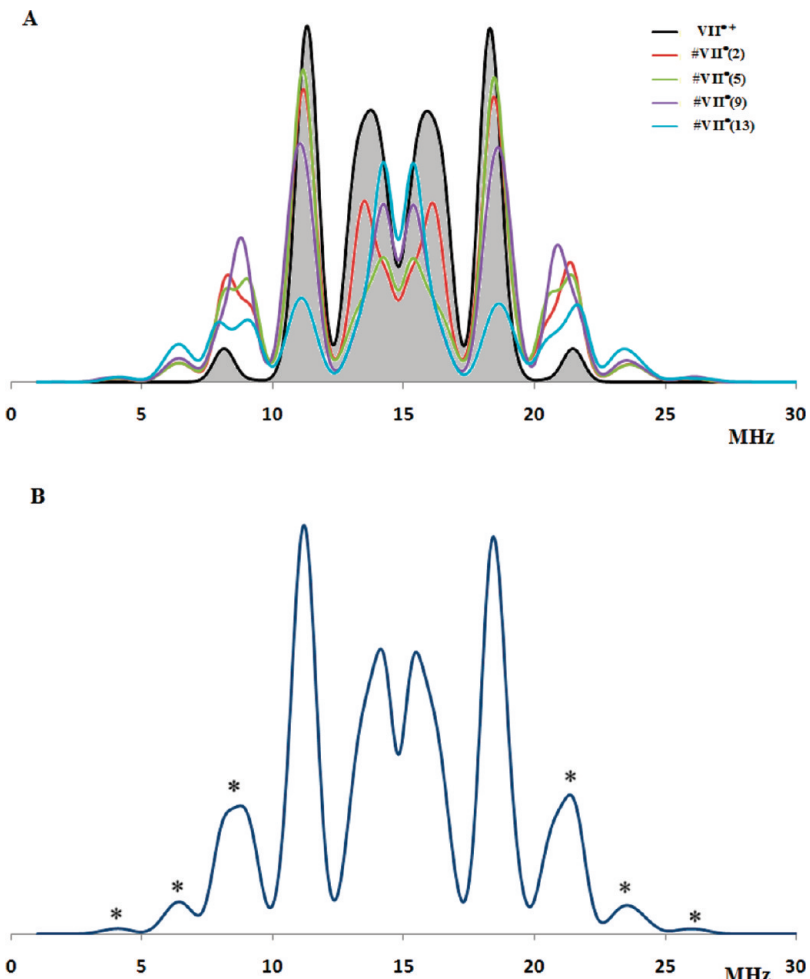


Figure 9. (A) Individual contribution of spirilloxanthin radicals (VII) to the Mims ENDOR spectrum; VII*+ is indicated by the gray shaded area, #VII*(2) by red, #VII*(5) by green, #VII*(9) by purple, and #VII*(13) by blue lines. (B) Simulated Mims ENDOR spectrum of the sum of spirilloxanthin radicals VII*+, #VII*(2), #VII*(5), #VII*(9), and #VII*(13) in 1:1:1:1:1 ratio. Note: the outer peaks indicated by * are due to the neutral radicals.

The practical use of the DFT calculations to analyze mixtures of carotenoid radicals produced by irradiation on an artificial matrix is demonstrated. The Mims ENDOR spectra of lycopene (**II**) radicals on silica–alumina (Figure 11) were measured as a function of τ (in Figure 11A, $\tau = 220$ ns; in Figure 11B, $\tau = 120$ ns), and the spectra were simulated using the hyperfine coupling constants determined from DFT and listed in the Supporting Information. Pulsed ENDOR spectra were measured at different delay times τ because the ENDOR amplitude has periodic oscillations known as “blind spots” at the hyperfine splitting A , proportional to $1 - \cos(2\pi A\tau)$.²³ Powder Mims ENDOR spectra exhibit resolved features that can be simulated using the full tensor (anisotropic and isotropic components found in the Supporting Information in Tables S7–S11) of the radical cation and the favorable neutral radicals. The radical anion has similar couplings to the radical cation and was not included in the simulation. (See Tables S7 and S12 in the Supporting Information.) The fit at the outer edges is diagnostic for neutral radicals because the edges contain contributions from only the neutral radicals, denoted as*. The blue curve includes these neutral radical species and account for the outer edges, agreeing with the experimental spectrum in red. The spectral lines in the

center of Mims ENDOR spectra are due to the matrix protons, which were not included in the simulation. The Mims ENDOR simulation does show in Figure 11 hyperfine couplings greater than 15 MHz (the maximum value of the isotropic couplings for the radical cation is 7.95 MHz) from the methyl groups in each neutral radical. These large couplings from the individual neutral radicals are required for the Mims ENDOR lines above 22.5 MHz and below 7.5 MHz, along with a small contribution from large anisotropic couplings.

Similar experimental Mims ENDOR spectra have been reported for the lutein radicals,¹³ astaxanthin radicals,²⁵ canthaxanthin,²⁶ and the 9'-*cis*-neoxanthin radicals.¹¹ These spectra can be compared with Figures 9–11 and used as a guide for detecting similar carotenoid radicals by Mims ENDOR measurements. The hyperfine coupling tensors given in the Supporting Information can be used to simulate ENDOR spectra, both Mims and Davies, and to estimate the appropriate τ for the Mims experiment to be used for a given combination of carotenoid radical cations, neutral radicals, and anions. The simulated spectra can be used as a guide to prove or disapprove the presence of these radicals.

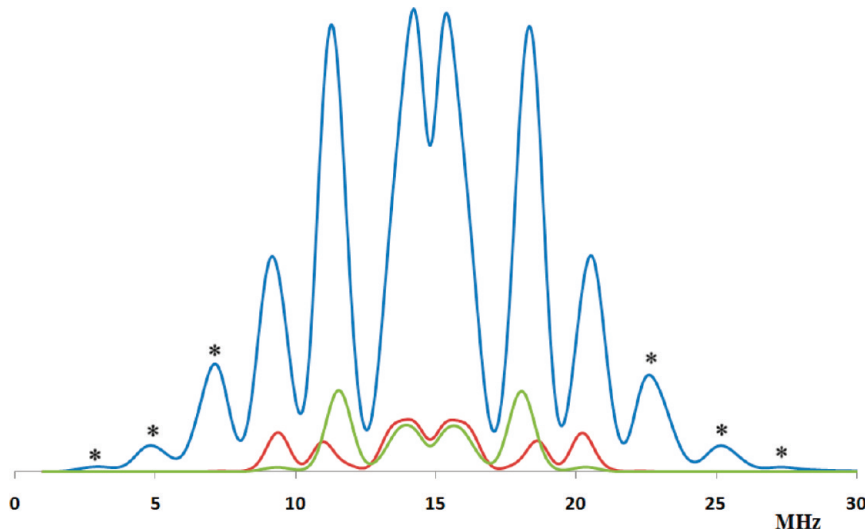


Figure 10. Simulated Mims ENDOR spectrum of neurosporene (**III**) radicals (in blue) $\tau = 220$ ns, $B = 3475$ G, mw = 9.76 GHz, and $\nu_n = 14.79$ MHz using the hyperfine coupling tensors given in the Supporting Information. The blue plot is the simulation of $\text{III}^{\bullet+}$, $\text{III}^{\bullet-}(34)$, $\text{III}^{\bullet-}(3'4')$, $\text{III}^{\bullet-}(7'8')$, # $\text{III}^{\bullet}(4)$, # $\text{III}^{\bullet}(5)$, # $\text{III}^{\bullet}(9)$, # $\text{III}^{\bullet}(13)$, # $\text{III}^{\bullet}(8')$, # $\text{III}^{\bullet}(9')$, and # $\text{III}^{\bullet}(13')$ radicals in equal amounts. The red plot is the simulation of the radical cation $\text{III}^{\bullet+}$; the green plot is the simulation of the radical anions $\text{III}^{\bullet-}(34)$, $\text{III}^{\bullet-}(3'4')$, and $\text{III}^{\bullet-}(7'8')$. Note: the outer peaks indicated by * are due to the neutral radicals.

■ DISCUSSION

Crystal Structure Examination. The proton loss ability has significant implications for the crystal structure or spatial arrangements of the biological systems in which these carotenoids occur. Following the formation of a carotenoid radical when a charge-transfer occurs¹⁰ between $\text{Car}^{\bullet+}$ and $\text{Chl}^{\bullet-}$, proton loss would make it possible to generate neutral radicals. Formation of the radical cation will depend on the location of the charge transfer state relative to the excited states of the system.⁵ According to the crystal structure of LH2 from *Rs. molischianum*,¹ one end of lycopene **II** lies outside the membrane near the aqueous surface and among potential proton acceptors, whereas the opposite end is in van der Waals contact with the BChl molecules. Under strong illumination, carotenoid radical cation $\text{II}^{\bullet+}$ is in position to deprotonate at the C4 end outside the membrane to create a neutral radical. Delocalization of the spin would place some spin density near the BChl at the other end, helping quench subsequent excited BChl. Proton loss from C5, C9, and C13-methyl groups along the chain would be suppressed because of the hydrophobic surroundings and because of the high energy for loss at these positions. Thus, **II** may play a dual role in energy transfer¹ at low light and in photoprotection at high light.

Our DFT calculations suggest an explanation for the different amount of carotenoid radicals observed in LH2 from *Rb. sphaeroides*.⁴ No radicals were observed for **V** in LH2, whereas they were observed with **III** (10–15%) and **IV** (5–8%). **III** and **IV** radical cations can readily deprotonate from C4 or C2 methylene groups at the polar end, whereas deprotonation is blocked by the carbonyl group for **V**. According to the most recent crystal structure of LH2,^{8,9} the polar end of the carotenoids lies in hydrophilic pockets on both surfaces of the membrane, whereas the rest of the carotenoid chain is buried in the membrane and is unlikely to deprotonate to form a longer-lived radical. Therefore, we would expect that **III** and **IV** would have higher yield of long-lived radicals than **V**. This trend parallels that predicted from calculations of energy transfer states.⁵

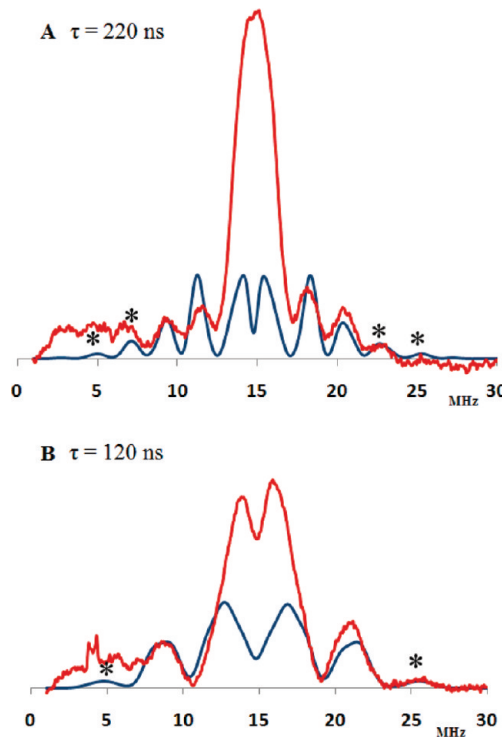


Figure 11. Pulsed Mims ENDOR spectra of lycopene (**II**) radicals as a function of τ . (A) 220 ns and (B) 120 ns. The red trace is the experimental spectrum produced in activated silica–alumina after UV irradiation. ENDOR parameters: $T = 20$ K, $B = 3475$ G, and $\nu = 9.764$ GHz. The blue trace is the simulated spectrum using isotropic and anisotropic DFT-calculated couplings listed in Tables S7–S11 of the Supporting Information for $\text{II}^{\bullet+}$, # $\text{II}^{\bullet}(4)$, # $\text{II}^{\bullet}(5)$, # $\text{II}^{\bullet}(9)$, and # $\text{II}^{\bullet}(13)$ in a 1:1:1:1 ratio. Note: ENDOR lines occur at $\nu_n = \pm A/2$, where ν_n is the proton frequency situated at the center of the ENDOR spectrum (proton frequency, $\nu_n = 14.793571$ MHz). Note: the outer peaks indicated by * are due to the neutral radicals. Below 6 MHz, the baseline includes an artifact from the nonlinearity of the ENDOR amplifier and thus interferes with low-frequency ENDOR lines due to neutral radicals.

In RC from *Rb. sphaeroides*,² IV occurs as the 15'-cis configuration; the carotenoid does not lie across the membrane but is near BChl and aromatic amino acid side chains. Proton loss would not occur in this situation even if a radical cation is formed because good proton acceptors are absent near IV. This location explains why IV efficiently quenches the triplet of the RC BChl but not its singlet state.

CONCLUSIONS

Losing a proton from a methylene group at the end of conjugation of the radical cation forms neutral radicals that extend the conjugated system, with the spin delocalized over the whole π -conjugated system. Using data presented here, we were able to determine what functions the carotenoids might serve based on their properties and location in photosynthetic media. Loss of protons from C4 or C4' methylene positions of II^{•+} could potentially occur because of the orientation of II in the LH2 of *Rs. molischianum*. Loss of protons from the radical cations of III, IV, and V in LH2 will depend on the bacterial species, the chemical nature of the carotenoid, and the location of the charge transfer state. Proton loss from the radical cation can occur from either end for a symmetric carotenoid such as VII, but for the asymmetric carotenoid VI, proton loss depends on the location of its polar end.

Carotenoid neutral radicals generated by proton loss from the radical cation of the fully conjugated carotenoid bisdehydrolycopenoate with conjugation length $n = 15$ can occur from any of the methyl groups, but it is preferred for the methyl group at C1(1') position by 8 to 9 kcal/mol. Decreasing the conjugation length to $n = 11$ (lycopene) by saturation of the double bonds C3-C4 and C3'-C4' results in a preferred proton loss at C4 or C4' methylene groups but less favorable by 5, 11, and 11.3 kcal/mol at C5(5'), C9(9'), and C13(13')-methyl groups. Saturation at C7'-C8' decreases the conjugation length to $n = 9$, 10, and 11 (neurosporene, spheroidene-methoxy at C1, and spheroidenone-methoxy at C1 and carbonyl at C2), resulting in the formation of a neutral radical, being the most favorable at C8' methylene group. Adding a methoxy group at C1 and keeping the double bond at C7'-C8' increases the conjugation to $n = 12,13$ (anhydrorhodovibrin, spirilloxanthin), and proton loss is favored at C2 instead of C8' methylene group. Adding a carbonyl at C2 (spheroidenone) prevents loss at C2, and thus loss is favored at C8' methylene group. A smooth relationship exists between the number of carbon atoms over which the unpaired spin density is distributed versus the relative energies for the loss of protons from the radical cations.

Mims ENDOR spectra have been simulated for the various radicals that can be formed for open chain linear carotenoids enabling their identification. The ability to block or allow formation of long-lived neutral radicals by simple alteration of the linear carotenoids and their environment allow them to participate in a wide range of transfer and energy quenching roles in biological or photochemical energy transductions.

ASSOCIATED CONTENT

Supporting Information. Calculated hyperfine coupling tensors for carotenoid radicals I–VII using B3LYP/TZP-(Ahlrichs)/B3LYP/6-31G**; A_{XX} , A_{YY} , A_{ZZ} , anisotropic coupling tensors for α -protons; A_{iso} , isotropic coupling constants, bold values are for β -methyl protons; relative energy $\Delta E(n)$ versus the

delocalization length N using the values in Table 1. This material is available free of charge via the Internet at <http://pubs.acs.org>.

AUTHOR INFORMATION

Corresponding Author

*E-mail: lkispert@bama.ua.edu.

ACKNOWLEDGMENT

This work was supported in part by The Chemical Sciences, Geosciences and Biosciences Division, Office of Basic Sciences, U.S. Department of Energy, grant DEFG02-86ER-13465 (L.D. K.), by the Natural Science Foundation for EPR instrument grants CHE-0342921 and CHE-0079498, and by the National Institute of Health, grant GM61904 (M.K.B.). This work was partially carried out using the resources provided by the Alabama Supercomputer Center in Huntsville, Alabama. For computer facilities, we thank Professor David Dixon who is indebted to the Robert Ramsay Endowment of the University of Alabama and to the Department of Energy. This study on part of the Hungarian authors was supported by the Hungarian National Research Foundation (OTKA K 76176 and K 83898).

REFERENCES

- (1) Koepke, J.; Hu, X.; Muenke, C.; Schulten, K.; Michel, H. *Structure* **1996**, *4*, 581–597.
- (2) Qian, P.; Saiki, K.; Mizoguchi, T.; Hara, K.; Sashima, T.; Fujii, R.; Koyama, Y. *Photochem. Photobiol.* **2001**, *74*, 444–452.
- (3) Yeliseev, A. A.; Eraso, J. M.; Kaplan, S. *J. Bacteriol.* **1996**, *178*, 5877–5883.
- (4) Polivka, T.; Pullerits, T.; Frank, H. A.; Cogdell, R. J.; Sundstrom, V. *J. Phys. Chem. B* **2004**, *108*, 15398–15407.
- (5) Wormit, M.; Harbach, P. H.; Mewes, J. M.; Amarie, S.; Wachtveitl, J.; Dreuw, A. *Biochim. Biophys. Acta* **2009**, *1787*, 738–746.
- (6) Gall, A.; Cogdell, R. J.; Robert, B. *Biochemistry* **2003**, *42*, 7252–7258.
- (7) McDermott, G.; Prince, S. M.; Freer, A. A.; Hawthornthwaite-Lawless, A. M.; Papiz, M. Z.; Cogdell, R. J.; Isaacs, N. W. *Nature* **1995**, *374*, 517–521.
- (8) Papiz, M. Z.; Prince, S. M.; Howard, T.; Cogdell, R. J.; Isaacs, N. W. *J. Mol. Biol.* **2003**, *326*, 1523–1538.
- (9) Prince, S. M.; Papiz, M. Z.; Freer, A. A.; McDermott, G.; Hawthornthwaite-Lawless, A. M.; Cogdell, R. J.; Isaacs, N. W. *J. Mol. Biol.* **1997**, *268*, 412–423.
- (10) Holt, N. E.; Zigmantas, D.; Valkunas, L.; Li, X. P.; Niyogi, K. K.; Fleming, G. R. *Science* **2005**, *307*, 433–436.
- (11) Focsan, A. L.; Molnar, P.; Deli, J.; Kispert, L. *J. Phys. Chem. B* **2009**, *113*, 6087–6096.
- (12) Focsan, A. L.; Bowman, M. K.; Konovalova, T. A.; Molnar, P.; Deli, J.; Dixon, D. A.; Kispert, L. D. *J. Phys. Chem. B* **2008**, *112*, 1806–1819.
- (13) Lawrence, J.; Focsan, A. L.; Konovalova, T. A.; Molnar, P.; Deli, J.; Bowman, M. K.; Kispert, L. D. *J. Phys. Chem. B* **2008**, *112*, 5449–5457.
- (14) Gao, Y. L.; Shinopoulos, K. E.; Tracewell, C. A.; Focsan, A. L.; Brudvig, G. W.; Kispert, L. D. *J. Phys. Chem. B* **2009**, *113*, 9901–9908.
- (15) Hideg, E.; Barta, C.; Kalai, T.; Vass, I.; Hideg, K.; Asada, K. *Plant Cell Physiol.* **2002**, *43*, 1154–1164.
- (16) Frisch, M. J.; Trucks, G. W.; Schlegel, H. B.; Scuseria, G. E.; Robb, M. A.; Cheeseman, J. R.; Montgomery, J. A., Jr.; T., V.; Kudin, K. N.; Burant, J. C.; Millam, J. M.; Iyengar, S. S.; Tomasi, J.; Barone, V.; Mennucci, B.; Cossi, M.; Scalmani, G.; Rega, N.; Petersson, G. A.; Nakatsuji, H.; Hada, M.; Ehara, M.; Toyota, K.; Fukuda, R.; Hasegawa, J.; Ishida, M.; Nakajima, T.; Honda, Y.; Kitao, O.; Nakai, H.; Klene, M.; Li, X.; Knox, J. E.; Hratchian, H. P.; Cross, J. B.; Adamo, C.; Jaramillo, J.; Gomperts, R.; Stratmann, R. E.; Yazyev, O.; Austin, A. J.; Cammi, R.;

Pomelli, C.; Ochterski, J. W.; Ayala, P. Y.; Morokuma, K.; Voth, G. A.; Salvador, P.; Dannenberg, J. J.; Zakrzewski, V. G.; Dapprich, S.; Daniels, A. D.; Strain, M. C.; Farkas, O.; Malick, D. K.; Rabuck, A. D.; Raghavachari, K.; Foresman, J. B.; Ortiz, J. V.; Cui, Q.; Baboul, A. G.; Clifford, S.; Cioslowski, J.; Stefanov, B. B.; Liu, G.; Liashenko, A.; Piskorz, P.; Komaromi, I.; Martin, R. L.; Fox, D. J.; Keith, T.; Al-Laham, M. A.; Peng, C. Y.; Nanayakkara, A.; Challacombe, M.; Gill, P. M. W.; Johnson, B.; Chen, W.; Wong, M. W.; Gonzalez, C.; Pople, J. A. *Gaussian 03*; Gaussian, Inc.: Wallingford, CT, 2004.

- (17) Becke, A. D. *J. Chem. Phys.* **1993**, *98*, 5648–5652.
- (18) Lee, C. T.; Yang, W. T.; Parr, R. G. *Phys Rev B* **1988**, *37*, 785–789.
- (19) Gao, Y. L.; Focsan, A. L.; Kispert, L. D.; Dixon, D. A. *J. Phys. Chem. B* **2006**, *110*, 24750–24756.
- (20) Schafer, A.; Horn, H.; Ahlrichs, R. *J. Chem. Phys.* **1992**, *97*, 2571–2577.
- (21) Cho, H.; Felmy, A. R.; Craciun, R.; Keenum, J. P.; Shah, N.; Dixon, D. A. *J. Am. Chem. Soc.* **2006**, *128*, 2324–2335.
- (22) Semichem, Inc. <http://www.semichem.com/ampac/ampacgui-features.php>. Accessed 07/06/2011.
- (23) Mims, W. B. *Proc. R. Soc. London, Ser. A* **1965**, *283*, 452–457.
- (24) Astashkin, A. U. o. A. http://quiz2.chem.arizona.edu/epr/epr_000006.htm. Accessed 07/06/2011.
- (25) Polyakov, N. E.; Focsan, A. L.; Bowman, M. K.; Kispert, L. D. *J. Phys. Chem. B* **2010**, *114*, 16968–16977.
- (26) Konovalova, T. A.; Li, S.; Polyakov, N. E.; Focsan, A. L.; Dixon, D. A.; Kispert, L. D. *J. Phys. Chem. B* **2009**, *113*, 8704–8716.